

Using ^{137}Cs and $^{210}\text{Pb}_{\text{ex}}$ to investigate the soil erosion and accumulation moduli on the southern margin of the Hunshandake Sandy Land in Inner Mongolia

HU Yunfeng^{1,2}, ZHANG Yunzhi^{1,2}

1. State Key Laboratory of Resources and Environmental Information System, Institute of Geographic Sciences and Natural Resources Research, CAS, Beijing 100101, China;

2. College of Resources and Environment, University of Chinese Academy of Sciences, Beijing 100049, China

Abstract: Wind-driven soil erosion results in land degradation, desertification, atmospheric dust, and sandstorms. The Hunshandake Sandy Land, an important part of the Two Barriers and Three Belts project, plays important roles in preventing desert and sandy land expansion and in maintaining local sustainability. Hence, assessing soil erosion and soil accumulation moduli and analyzing the dynamic changes are valuable. In this paper, Zhenglan Banner, located on the southern margin of the Hunshandake Sandy Land, was selected as the study area. The soil erosion and accumulation moduli were estimated using the ^{137}Cs and $^{210}\text{Pb}_{\text{ex}}$ composite tracing technique, and the dynamics of soil erosion and soil accumulation were analyzed during two periods. The results are as follows: (1) the regional ^{137}Cs reference inventory was $2123.5 \pm 163.94 \text{ Bq/m}^2$, and the regional $^{210}\text{Pb}_{\text{ex}}$ reference inventory was $8112 \pm 1787.62 \text{ Bq/m}^2$. (2) Based on the ^{137}Cs isotope tracing analysis, the erosion moduli ranged from -483.99 to $740.31 \text{ t} \cdot \text{km}^{-2} \cdot \text{a}^{-1}$. Based on the $^{210}\text{Pb}_{\text{ex}}$ isotope tracing analysis, the erosion moduli ranged from -441.53 to $797.98 \text{ t} \cdot \text{km}^{-2} \cdot \text{a}^{-1}$. (3) Compared with the earliest 50 years, the subsequent 50 years exhibited lower soil erosion moduli and accumulation moduli. Therefore, the activities of local sand dunes weakened, and the quality of the local ecological environment improved. The multi-isotope composite tracing technique combining the tracers ^{137}Cs and $^{210}\text{Pb}_{\text{ex}}$ has potential for similar soil erosion studies in arid or semiarid regions around the world.

Keywords: wind erosion; isotope tracing; reference inventory; quantitative estimation; sandy land

1 Introduction

Wind-driven soil erosion results in land degradation, desertification, atmospheric dust, and

Received: 2018-11-10 **Accepted:** 2019-02-15

Foundation: Strategic Priority Research Program of CAS, No.XDA19040301, No.XDA20010202; National Key Research and Development Program of China, No.2016YFC0503701, No.2016YFB0501502; Key Project of High-resolution Earth Observation, No.00-Y30B14-9001-14/16

Author: Hu Yunfeng (1974–), Associate Professor, specialized in environment monitoring & assessment and regional sustainable development. E-mail: huyf@lreis.ac.cn

sandstorms (Nan *et al.*, 2014). The southern margin of the Hunshandake (Otindag) Sandy Land is located in southeastern Inner Mongolia, China, and is a major part of the Two Barriers and Three Belts project, which was implemented by the Chinese National Major Function Oriented Zoning Plan. This region plays important roles in preventing the expansion of the Hunshandake Sandy Land and enhancing the extent of sandy grassland. This work is important not only for local ecological security and sustainable development but also for guaranteeing the ecological quality in surrounding regions, such as the capital Beijing, and throughout northern China (He *et al.*, 2015). Hence, assessment of the soil erosion and soil accumulation moduli and analysis of the dynamic changes in this region are valuable.

The use of the ^{137}Cs tracer, including the quantitative evaluation method and associated model, in soil erosion application studies is relatively mature, and this technique has been applied for a long time worldwide (Feng *et al.*, 2011; Li *et al.*, 2011). However, since ^{137}Cs is derived from atmospheric nuclear blasts, its characteristics, including a single source, a lack of supplies, and a short half-life (30.17 a), make ^{137}Cs increasingly difficult to detect in soil samples. Researchers have to search for alternative isotopes, such as $^{210}\text{Pb}_{\text{ex}}$ or ^7Be or ^{10}Be , as soil tracers in soil erosion studies. ^{210}Pb is one isotope of the ^{238}U decay series and has a half-life of 22.26 years. Its parent isotope ^{222}Rn (half-life 3.8 d) is an inert gas and is derived from the decay of ^{226}Ra (half-life 1622 a) in natural soils and rocks. A portion of ^{222}Rn is transported to the atmosphere along soil pores and rock fissures. ^{210}Pb is released by the α decay of ^{222}Rn in the atmosphere, settles back to the ground surface, and is finally adsorbed by surface soil particles. This fraction of ^{210}Pb is called “noncarrier ^{210}Pb ” (labeled $^{210}\text{Pb}_{\text{ex}}$). When the ^{222}Rn that did not escape to the atmosphere decays to ^{210}Pb in the soil, it is also adsorbed by the soil. This fraction of ^{210}Pb is then called “compensatory ^{210}Pb ” (labeled $^{210}\text{Pb}_{\text{sup}}$) (Baskaran, 2016). Both ^{137}Cs and $^{210}\text{Pb}_{\text{ex}}$ have similar characteristics in that they are only adsorbed by soil particles and are rarely carried by rainwater or taken up by plants. The changes of ^{137}Cs or ^{210}Pb particles are only related to the physical migration of soil particles. This distinct property allows ^{137}Cs and $^{210}\text{Pb}_{\text{ex}}$ to be used as tracers in soil erosion and soil accumulation / deposition processes.

Many studies have been carried out using isotope tracers. Typical studies include determining regional reference inventories, understanding the migration process of tracers, constructing erosion modulus estimation models, and many case applications (Li *et al.*, 2009; Wang, 2010; Chappell *et al.*, 2012; Evans *et al.*, 2017). However, most previous studies have concentrated on water erosion processes and water erosion regions, and few studies have focused on wind erosion. Additionally, most previous studies have only applied single isotopes (such as ^{137}Cs or ^{210}Pb), and few studies have explored multi-isotope composite tracing techniques. Furthermore, there are few studies in sandy grassland or sandy land, which are the most common land types on the Mongolia Plateau and in the arid or semiarid regions of the Eurasia continent (Liu *et al.*, 2007; Qi *et al.*, 2008).

Zhenglan Banner, located on the southern margin of the Hunshandake Sandy Land, is a typical wind erosion zone on the Mongolia Plateau (Figure 1). Zhenglan Banner is also on the southern margins of the Hunshandake Sandy Land, which is invading southward into Zhenglan Banner. The regional land types are mainly grassland, sandy grassland and sandy land. Zhenglan Banner has experienced extremely complicated land use and land cover change processes, including grassland reclamation, cropland abandonment, grassland overgrazing, sand dune activation, sand dune solidification and many combinations of processes.

Additionally, soil samples obtained after the 21st century have a low ^{137}Cs activity, making the ^{137}Cs signal difficult to detect. The background plots (plots without erosion or accumulation) are easily contaminated due to frequent sandstorms and comprehensive land changes. Hence, it is difficult to determine the background plots or reference plots. All of these factors make the soil erosion quantitative assessment only using ^{137}Cs technique more uncertain.

According to the above considerations, based on traditional quantitative soil erosion studies using a single isotope (^{137}Cs), the authors introduced the $^{210}\text{Pb}_{\text{ex}}$ isotope tracing technique and carried out ^{137}Cs and $^{210}\text{Pb}_{\text{ex}}$ composite tracing analysis. The application of the composite isotope tracing method not only allows us to estimate the long-term (100 a) soil erosion modulus but also helps to reduce the uncertainties of the traditional methodology in background plot selection, regional reference inventory determination, and soil erosion modulus estimation. In addition, the combination of the two isotopes also helps us to compare the soil erosion processes in two different periods and obtain more in-depth soil erosion modulus information.

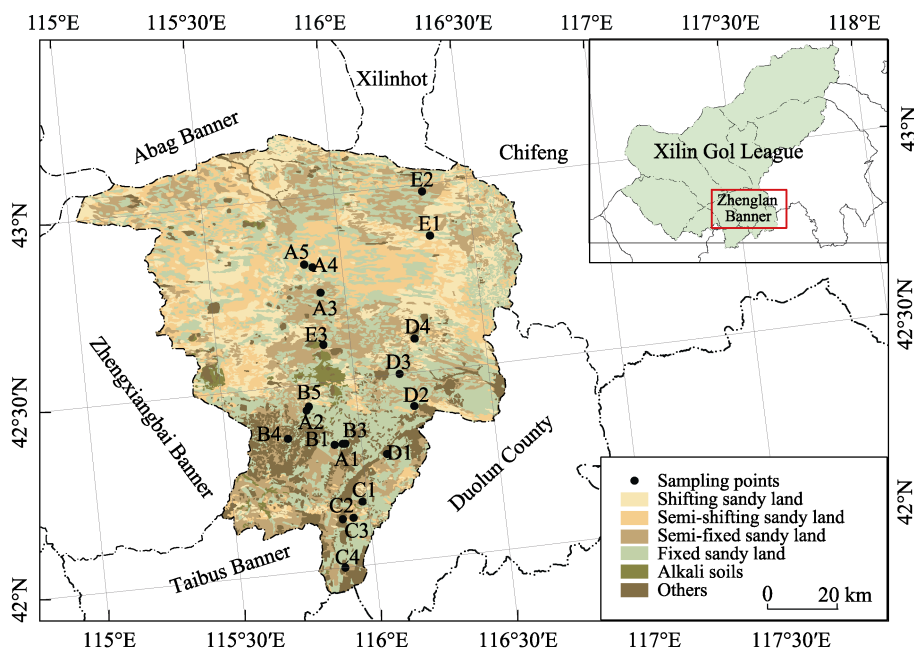


Figure 1 The spatial distributions of plots and land in Zhenglan Banner, Xilin Gol, Inner Mongolia

2 Study area

The Zhenglan Banner of Xilin Gol League was selected as our study region. The study region lies between $115^{\circ}00'–116^{\circ}42'E$ and $41^{\circ}59'–43^{\circ}11'N$ and is adjacent to Duolun County and Chifeng City to the east, bordering Zhengxiangbai Banner to the west, Abag Banner and Xilinhot City to the north, and Taipusi Banner and Hebei Province to the south (Figure 1). The study area has a temperate continental monsoon climate. The annual average precipitation is about 365 mm, the annual average evaporation is about 1925 mm, and the annual average wind speed is about 4.3 m/s. Springs are windy and dry, summers are warm and short, autumns are cool, and winters are cold and long. Temperature and precipitation change considerably over the course of a year (Li *et al.*, 2013). The Hunshandake Sandy Land covers

the northern part of Zhenglan Banner. From north to south, the region is composed of sandy vegetation and typical grassland vegetation. The whole area is dominated by hilly sandy grassland, and there is intrazonal meadow vegetation in some regions (Li *et al.*, 2011).

3 Sampling and testing

Two north-south belt transects have been established in Zhenglan Banner. The belt transects are specifically designed along the invasion direction of the Hunshandake Sandy Land. In total, 21 sampling points were positioned every 10–20 km along the belt transects, and the specific location of each soil sampling plot was further determined according to the local topography, soil type, land use history and vegetation coverage.

It is critical to select reliable background plots to determine the regional reference inventories of ^{137}Cs and $^{210}\text{Pb}_{\text{ex}}$ in isotope tracing studies. The land use history and sandstorm activities in this region are so complicated that the traditional selection standards based on high-coverage grassland or long-term cultivated land become difficult to apply without auxiliary information. We used the long-term Chinese land use and land cover database (1990–2015) (provided by the Institute of Geographic Sciences and Natural Resources Research of the Chinese Academy of Sciences) and on-site observations of vegetation coverage. We primarily selected 13 grassland plots as potential background plots that have maintained high coverage since the 1990s. Another 8 plots were regarded as erosion sites because they experienced changes in land cover/land use type during the past 35 years. At each site, 4 suites of soil samples were collected according to a triangle sampling layout: 3 full-profile samples were excavated at the vertexes of the triangle, and a suite of layer samples were collected at the center. The full-profile samples were taken using a soil driller with an internal diameter of 35 mm and a maximum sampling depth of 30 cm. For the layer samples, a layer thickness of 3 cm was used for the top 0–15 cm column, a layer thickness of 5 cm was used for the 15–20 cm column, and a thickness of 10 cm was used for the lowermost 20–30 cm column.

Isotope activity measurements were performed at the Laboratory of Radiation and Environment of China University of Geosciences (Beijing). Before the instrument measurements, all soil samples were sealed for 1 week to achieve a decay balance between ^{210}Pb and its parent isotope. The isotope activity was measured by a detector (BE3830, produced by ORTEC, USA) with high-purity germanium and wide energy bands. The test process followed the national standard of the γ -ray spectrum analysis for soil radionuclides (GB 11743–2013). The duration of each measurement was $\geq 25,000$ s. The energy resolution of the detector was 2.25 MeV at ^{60}Co 1.33 MeV, and the peak-to-Compton Ratio was $>60:1$, indicating good stability. The channel drift was $<1/\text{month}$, the relative detection efficiency was 62%, and the relative error of repeated tests was $<10\%$. ^{137}Cs activity can be calculated from the full peak area of the 661.7 keV ray. The $^{210}\text{Pb}_{\text{ex}}$ activity is equal to the value from the full peak area of the 46.5 keV ray (^{210}Pb activity) minus the full peak area of the ray at 351.9 keV (^{226}Ra activity).

The activity information obtained from the instrument measurements is the activity value per unit mass (Bq/kg). In soil isotope tracing studies, such activity values need to be converted to area-based cumulative activity, which is summed from the surface to the depth at which the isotopes are completely undetectable.

For the layer samples, the total amount of ^{137}Cs or $^{210}\text{Pb}_{\text{ex}}$ can be calculated from the fol-

lowing formula:

$$CPI(PPI) = \sum_{i=1}^n 1000 * C_i * B_i * D_i \quad (1)$$

where CPI (^{137}Cs point inventory) is the total content of ^{137}Cs , PPI ($^{210}\text{Pb}_{\text{ex}}$ point inventory) is the total content of $^{210}\text{Pb}_{\text{ex}}$ (Bq/m^2), i is the layer number, n is the amount of sampling layers in each layer sample suite, C_i is the isotope activity (Bq/kg) of ^{137}Cs or $^{210}\text{Pb}_{\text{ex}}$ in the i -th layer sample, B_i is the bulk density (g/cm^3) of the i -th layer, and D_i is the sampling depth (m) of the i -th layer.

For the full-profile samples, the total amount of ^{137}Cs or $^{210}\text{Pb}_{\text{ex}}$ can be calculated by the following formula:

$$CPI(PPI) = C_i * W / S \quad (2)$$

where C_i represents the isotope activity (Bq/kg) of ^{137}Cs or $^{210}\text{Pb}_{\text{ex}}$ in the whole sample, W is the total weight (kg) of each soil sample after sieving, and S is the cross-sectional area (m^2) of the soil driller.

4 Results and analysis

4.1 ^{137}Cs and ^{210}Pb reference inventory

The reference inventory (CRI: ^{137}Cs reference inventory; PRI: ^{210}Pb reference inventory) refers to the activity of ^{137}Cs or $^{210}\text{Pb}_{\text{ex}}$ in the sample without soil erosion, accumulation/deposition, or any kind of external disturbances. Determining a reliable and accurate CRI or PRI is a key step in the estimation of the soil erosion modulus. In an early-proposed method, one or a small number of background plots are selected through field investigations and on-site observations, and then the CPI (or PPI) or the mean CPI (or PPI) is regarded as the regional CRI (or PRI). With the development of isotope tracing techniques, especially with the development of large-scale erosion studies in northern China, Zhang *et al.* (1994) proposed a method for determining the CRI by investigating the isotope distribution characteristics along soil profiles. Qi *et al.* (2006) proposed a method of calculating the reference inventory using a theoretical model, and Hu *et al.* (2014) proposed a systematic method by combining model estimation result and isotope distribution characteristics. The above methods have proven to be efficient for studies in arable land or grassland. However, for sandy grassland that are characterized by complex land use and land cover changes and frequent sandstorm activities, a more cautious and complex approach is required to determine the background plots and the corresponding values of CRI and PRI.

Considering the relationship between the atmospheric deposition of ^{90}Sr and the amount of atmospheric rainfall, Waling and He (2000) developed a model to estimate the ^{137}Cs reference inventory globally by inputting the location information and the rainfall amount information:

$$A(\phi, \theta) = \frac{1.10 f_{h,z}(\phi_z) A_{h,b}(\theta_b) \left[\beta + \gamma \left(\frac{P}{P'} \right)^\delta \right]}{\alpha(\phi_z, \theta_b)} \quad (3)$$

where $A(\phi, \theta)$ is the ^{137}Cs reference inventory at the position (ϕ, θ) ; $f_{h,z}(\phi_z)$ is the ^{137}Cs change induced by the longitude difference (where $h=1$ refers to the northern hemisphere, $h=2$ refers to the southern hemisphere, $z=1-8$, and ϕ_z refers to the position index determined by the longitude value), and $A_{h,b}(\theta_b)$ is the ^{137}Cs change induced by the latitude dif-

ference (where $h=1$ indicates the northern hemisphere, $h=2$ indicates the southern hemisphere, $b=1-9$, and θ_b represents the position index defined by the latitude value); P indicates the annual average rainfall (mm) at the position (ϕ, θ); and $P'=1$ mm. β, γ and δ are constants of 0.15, 0.0051 and 0.45, respectively.

Qi *et al.* (2006) compared the model estimates with the measured CRI chosen by different researchers in China. Qi noted that the model normally underestimates the true CRI. Hu *et al.* (2014) further noted that the measured CRIs in Inner Mongolia are 120%–155% of the model estimates. According to the estimates of the module developed by Walling *et al.*, kindly provided by Qi *et al.*, and the amplification factor estimated by Hu *et al.*, the authors of this paper first calculated the potential CRI ranges. Then, the authors investigate the potential background plots one by one to check whether they fall within the of potential CRI ranges (Table 1).

Table 1 The model estimated value, potential CRI range and measured CPIs

Plot	Longitude (°E)	Latitude (°N)	Elevation (m)	Annual rainfall mm·a ⁻¹	Model esti- mated CRI Bq·m ⁻²	Potential CRI range Bq·m ⁻²	Measured CPI Bq·m ⁻²	Is the measured CPI fall within the potential CRI range?
A1	115.93	42.33	1367				2864	no
A3	115.91	42.74	1319				2225	yes
A4	115.89	42.81	1325				2022	yes
B1	115.9	42.33	1365				2455	yes
B2	115.9	42.33	1366				1928	yes
B3	115.94	42.33	1376				2124	yes
B4	115.73	42.36	1389	365	1576	1890–2665	2952	no
B5	115.82	42.44	1342				2394	yes
C2	115.9	42.13	1316				3256	no
C3	115.94	42.13	1339				2904	no
D1	116.09	42.29	1282				4635	no
D2	116.21	42.41	1280				1987	yes
D3	116.17	42.5	1426				3511	no

Table 1 shows that the CPI values of plots A3, A4, B1, B2, B3, B5, and D2 are within the potential CRI range. Through examining the ¹³⁷Cs distribution characteristics, we reach the following conclusions:

In plots A3 and A4, the maximum ¹³⁷Cs occurrence depths are 15 cm and 20 cm, respectively. The peak values of ¹³⁷Cs activity are 16.92 Bq/kg and 11.35 Bq/kg, respectively, both appearing at 9–12 cm. These values exhibit the typical distribution type characterized by “a single peak + a negative exponential curve”. This distribution pattern is normally related to the process of downward diffusion of ¹³⁷Cs from the surface to deeper layers after its deposition (Porto *et al.*, 2011). Therefore, plots A3 and A4 can be regarded as background plots.

In plots B1, B2, B5, and D2, although the ¹³⁷Cs distribution exhibits a negative exponential curve or “a single peak + a negative exponential curve”, the maximum occurrence depth of ¹³⁷Cs is very shallow. The depths at these sites are only 9 cm, 12 cm, 9 cm, and 6 cm, respectively, and these depths are much shallower than the normal occurrence depth of 15–25 cm (Winkelbauer *et al.*, 2012). Therefore, the above 4 plots should not be used as background plots, and they should be regarded as eroded plots.

In plot B3, the depth of ¹³⁷Cs occurrence is 20 cm, and the surface soil (0–3 cm) has the highest activity (28.01 Bq/kg). The ¹³⁷Cs activity decreases rapidly with increasing depth,

which is consistent with the typical ^{137}Cs distribution pattern in background plots (Zhang *et al.*, 1994; Hu *et al.*, 2014). Therefore, plot B3 can be used as a regional reference plot.

Table 1 also shows that the CPIs of plots A1, B4, C2, C3, D1, and D3 are not within the potential CRI range. Therefore, these plots are regarded as potential soil erosion plots or potential soil accumulation plots. By examining the profile of the ^{137}Cs distribution (Figure 3), we can conclude the following:

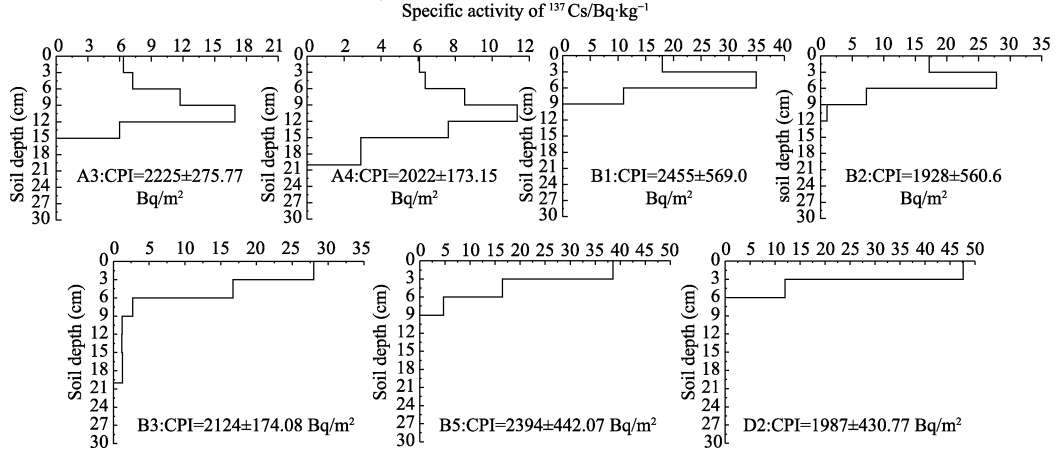


Figure 2 The ^{137}Cs distribution patterns and CPIs in potential reference plots

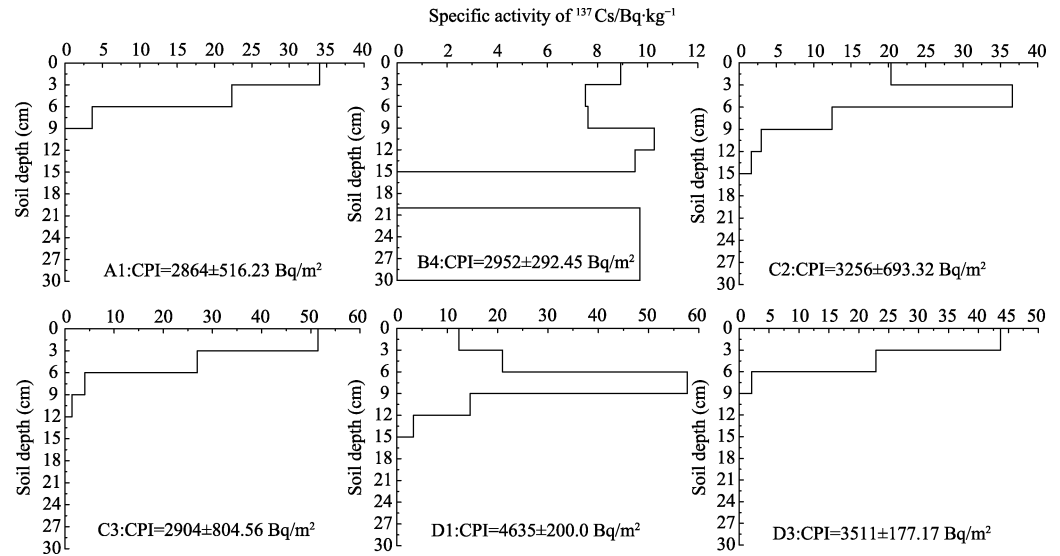


Figure 3 The ^{137}Cs distribution patterns and CPIs in potential erosion and accumulation plots

In the plots A1, C3 and D3, ^{137}Cs shows a negative exponential curve distribution, and the maximum depth of ^{137}Cs occurrence is 9 cm, 12 cm and 9 cm, respectively. The CPIs of all plots are higher than the upper bound of the potential CRI range (2665 Bq/m²) because the topsoil is rich in ^{137}Cs . These plots are concluded to be soil accumulation plots.

In the plot B4, there is no ^{137}Cs at 15–20 cm. The ^{137}Cs profile shows a uniform distribution above and below that depth. This is consistent with the typical ^{137}Cs distribution pattern in cultivated land. Hence, this plot is regarded as a plot that has inherited the characteristics of former cropland.

For plots C2 and D1, the maximum occurrence depth is 15 cm, and the CPI is significantly larger than the upper limit of the potential CRI range (2665 Bq/m²). The plots are thought to represent the accumulation of soil and sand in recent decades.

Because the study area is located on a high plain, the local topography has little influence on the settling of ¹³⁷Cs. Therefore, the regional ¹³⁷Cs reference inventory can be derived from the mean CPIs of multiple background plots (Liu *et al.*, 2010). In this study, three plots, i.e., A3, A4, and B3, have been selected as background plots. The regional CRI mean value and the mean square error are calculated from the CPI values of these 3 plots (involving 3 suites of layer samples and 9 full-profile samples). Finally, the regional CRI is determined to be 2123.5±163.94 Bq/m². The determined CRI is about 135% of the model estimate (1576 Bq/m²) and is consistent with the CRI range in previous studies in northern China and the Mongolia Plateau (Zhang *et al.*, 2015).

There are few studies on the selection of ²¹⁰Pb_{ex} background plots and the determination of ²¹⁰Pb_{ex} reference inventory. Although some estimation models are also based on the precipitation regression method, the accuracy of the estimated PRI requires further verification (Chen *et al.*, 2013; Hu *et al.*, 2017). In this study, the authors propose a new method to select the appreciate background plots. Extensive knowledge and on-site environmental characteristics are taken into account: the selection of ¹³⁷Cs background plots, the long-term history of land cover/land use change, the model-estimated value of CRI, the comparison of CRI in the adjacent regions, and the isotope distribution pattern within the soil profile. All the above information is used for the selection of the ²¹⁰Pb background plots. The determined reference points and reference inventory of ²¹⁰Pb_{ex} are thus more reliable. In this study, specifically, the background plots (A3, A4, and B3) determined in the ¹³⁷Cs study were also used as the ²¹⁰Pb_{ex} reference plots. The PRI of the southern margin of the Hunshandake Sandy Land was finally determined to be 8112±1787.62 Bq/m².

4.2 Erosion and accumulation modulus

Based on the characteristics of the ¹³⁷Cs amount and ¹³⁷Cs distribution within the soil profile in cultivated land and uncultivated land, Zhang *et al.* (1990) established a simplified mass balance model to measure the thickness of soil erosion/accumulation and the modulus of soil erosion/accumulation. The model is as follows:

$$X = X_0 \cdot e^{-\lambda \cdot h \cdot (T-1963)} \quad (4)$$

$$X_0 = CRI \cdot K \quad (5)$$

where X is the ¹³⁷Cs activity (Bq/m²); X_0 is the modified ¹³⁷Cs reference inventory (Bq/m²), which introduces wind and snow disturbance effects ($k=0.95$ (Sutherland, 1998)) to the original ¹³⁷Cs reference inventory; h is the annual average soil erosion thickness (cm/a); T is the sampling year; and λ is the morphological parameter of the ¹³⁷Cs distribution curve within the soil profile. The term λ can be obtained by the least squares fitting method.

The soil erosion modulus is calculated by the following formula:

$$E = 10000 \cdot B \cdot h \quad (6)$$

where E is the soil erosion modulus (t·km⁻²·a⁻¹) and B is the soil bulk density (t/m³).

According to the above formula, the soil erosion/accumulation modulus in each plot can be computed using the ¹³⁷Cs tracing technique (Table 2).

As shown in Table 2, the activities of ¹³⁷Cs in plots A1, B1, B4, B5, C2, C3, D1, and D3 are between 2394±442.07 and 4635±200.0 Bq/m². The CPIs of these plots are greater than

Table 2 ^{137}Cs activity and soil erosion/accumulation modulus estimated by the ^{137}Cs tracing technique

Plot	Soil	Topography	Vegetation coverage (%)	^{137}Cs activity (Bq/m^2)	Soil bulk density (t/m^3)	Erosion /accumulation thickness ($\text{mm}\cdot\text{a}^{-1}$)	Erosion /accumulation modulus ($\text{t}\cdot\text{km}^{-2}\cdot\text{a}^{-1}$)
A1	Chestnut soil	Fixed sandy land	70–80	2864±516.23	1.563	−0.144	−224.39
A2	Chestnut soil	Semifixed sandy land (gentle slope)	20–30	1332±857.16	1.587	0.170	269.79
A5	Aeolian sandy soil	Semifixed sandy land	30–40	591±256.27	1.472	0.503	740.31
B1	Chestnut soil	Fixed sandy land	70–80	2455±569.0	1.211	−0.080	−97.35
B2	Chestnut soil	Fixed sandy land	70–80	1929±560.6	1.309	0.018	24.21
B4	Chernozem	Fixed sandy land	70–80	2952±292.45	1.329	−0.156	−207.29
B5	Chestnut soil	Fixed sandy land	70–80	2394±442.07	1.335	−0.070	−93.67
C1	Chestnut soil	Fixed sandy land	30–40	1737±458.96	1.754	0.061	107.51
C2	Meadow soil	Fixed sandy land	70–80	3256±693.32	1.481	−0.196	−290.46
C3	Chestnut soil	Fixed sandy land	70–80	2904±804.56	1.567	−0.149	−233.85
C4	Chestnut soil	Fixed sandy land (hemidome)	40–50	1393±97.82	1.473	0.152	223.44
D1	Meadow soil	Fixed sandy land	70–80	4635±200.0	1.420	−0.341	−483.99
D2	Chestnut soil	Fixed sandy land	70–80	1987±430.77	1.488	0.006	9.19
D3	Chernozem	Fixed sandy land	70–80	3511±177.17	1.678	−0.227	−380.85
D4	Eolian sandy soil	Semifixed sandy land	30–40	1505±254.99	1.363	0.120	163.44
E1	Eolian sandy soil	Fixed sandy land (piedmont platform)	50–60	1451±339.53	1.712	0.135	231.16
E2	Eolian sandy soil	Semifixed sandy land	30–40	1401±139.49	1.672	0.149	249.71
E3	Meadow soil	Fixed sandy land (piedmont platform)	30–40	1859±222.90	1.632	0.034	54.81

the CRI and indicate the existence of sand accumulation in these plots. The accumulation rate of plot B5 is the lowest, i.e., $93.67 \text{ t}\cdot\text{km}^{-2}\cdot\text{a}^{-1}$. The accumulation rate of plot D1 is the highest, i.e., $483.99 \text{ t}\cdot\text{km}^{-2}\cdot\text{a}^{-1}$. The average annual accumulation thickness of all plots is $0.07\text{--}0.34 \text{ mm}\cdot\text{a}^{-1}$, and the erosion modulus is $93.67\text{--}483.99 \text{ t}\cdot\text{km}^{-2}\cdot\text{a}^{-1}$.

The ^{137}Cs activities in plots A2, A5, B2, C1, C4, D2, D4, E1, E2, and E3 are between 591 ± 256.27 and $1987\pm430.77 \text{ Bq/m}^2$, and the CPIs are less than the CRI, indicating soil erosion. Among them, plot D2 is located in the fixed sandy land, and it has the highest ^{137}Cs activity and the lowest annual erosion rate. In contrast, plot A5, which is located in semi-fixed sandy land, has the lowest ^{137}Cs activity and the highest annual erosion rate. The annual average erosion thickness ranges from $0.006\text{--}0.503 \text{ mm}\cdot\text{a}^{-1}$, and the erosion modulus varies from $9.19\text{--}740.31 \text{ t}\cdot\text{km}^{-2}\cdot\text{a}^{-1}$.

Unlike ^{137}Cs , $^{210}\text{Pb}_{\text{ex}}$, a natural radioisotope, continuously settles from the atmosphere to the surface soil. When the environment and soil erosion process are stable for a long time ($\geq 100 \text{ a}$), the $^{210}\text{Pb}_{\text{ex}}$ tracer in the soil achieves a steady state. Thus, $^{210}\text{Pb}_{\text{ex}}$ is generally considered to be able to measure the soil erosion modulus at the 100-year scale (Mabit *et al.*, 2008). Considering the continuous sedimentation process and the decay and loss processes of $^{210}\text{Pb}_{\text{ex}}$, Zhang *et al.* (2003) derived a mass balance model by measuring the steady distribution state of $^{210}\text{Pb}_{\text{ex}}$ in nonagricultural soils. Sun *et al.* (2013) simplified the model and established a new formula to depict the relationship between soil erosion rate and $^{210}\text{Pb}_{\text{ex}}$ content in uncultivated soil. The model is as follows:

$$I = (\lambda + 1 - e^{-\frac{h}{H}})A \quad (7)$$

$$I = \lambda A_{ref} \quad (8)$$

where I is the $^{210}\text{Pb}_{ex}$ sedimentation flux ($\text{Bq}/\text{m}^2 \cdot \text{a}^{-1}$), λ is the $^{210}\text{Pb}_{ex}$ decay coefficient, h is the annual erosion thickness ($\text{Bq}/\text{m}^2 \cdot \text{a}^{-1}$), H is the relaxation depth (kg/m^2), A is the $^{210}\text{Pb}_{ex}$ activity (Bq/m^2), and A_{ref} is the $^{210}\text{Pb}_{ex}$ reference inventory (Bq/m^2).

By combining formulas (7) and (8), the average annual erosion thickness in uncultivated soil can be derived as follows:

$$h = -H \ln \left(\lambda + 1 - \frac{\lambda A_{ref}}{A} \right) \quad (9)$$

According to the above formulas, the soil erosion/accumulation modulus using the $^{210}\text{Pb}_{ex}$ tracing technique can be obtained (Table 3).

Table 3 $^{210}\text{Pb}_{ex}$ activity and soil erosion/accumulation modulus estimated by $^{210}\text{Pb}_{ex}$ tracing technique

Plot	Soil	Topography	Vegetation coverage (%)	$^{210}\text{Pb}_{ex}$ activity (Bq/m^2)	Soil bulk density (t/m^3)	Erosion /accumulation thickness ($\text{mm} \cdot \text{a}^{-1}$)	Erosion /accumulation modulus ($\text{t} \cdot \text{km}^{-2} \cdot \text{a}^{-1}$)
A1	Chestnut soil	Fixed sandy land	70–80	9871±1298.12	1.563	−0.164	−255.87
A2	Chestnut soil	Semifixed sandy land (gentle slope)	20–30	6483±2885.46	1.587	0.232	368.74
A5	Aeolian sandy soil	Semifixed sandy land	30–40	7403±738.79	1.472	0.088	129.95
B1	Chestnut soil	Fixed sandy land	70–80	11151±159.99	1.211	−0.250	−302.74
B2	Chestnut soil	Fixed sandy land	70–80	7555±91.50	1.309	0.068	89.02
B4	Chernozem	Fixed sandy land	70–80	10174±1639.76	1.329	−0.186	−247.30
B5	Chestnut soil	Fixed sandy land	70–80	8118±930.08	1.335	−0.001	−0.90
C1	Chestnut soil	Fixed sandy land	30–40	6609±951.43	1.754	0.210	368.66
C2	Meadow soil	Fixed sandy land	70–80	12023±1286.46	1.481	−0.298	−441.53
C3	Chestnut soil	Fixed sandy land	70–80	7713±393.57	1.567	0.048	74.70
C4	Chestnut soil	Fixed sandy land (hemidome)	40–50	6461±1160.75	1.473	0.236	348.10
D1	Meadow soil	Fixed sandy land	70–80	9106±147.82	1.420	−0.100	−142.62
D2	Chestnut soil	Fixed sandy land	70–80	5143±662.26	1.488	0.536	797.98
D3	Chernozem	Fixed sandy land	70–80	9966±1698.73	1.678	−0.171	−286.75
D4	Aeolian sandy soil	Semifixed sandy land	30–40	5931±1660.60	1.363	0.341	464.27
E1	Aeolian sandy soil	Fixed sandy land (piedmont platform)	50–60	7270±783.81	1.712	0.107	182.98
E2	Aeolian sandy soil	Semifixed sandy land	30–40	6554±2132.22	1.672	0.220	367.25
E3	Meadow soil	Fixed sandy land (piedmont platform)	30–40	8871±673.03	1.632	−0.079	−128.53

As shown in Table 3, the $^{210}\text{Pb}_{ex}$ activities in plots A1, B1, B4, B5, C2, D1, D3, and E3 are between 8118±930.08 and 12023±1286.46 Bq/m^2 , and the PPIs are greater than the PRI, indicating soil accumulation. Among these plots, the annual accumulation rate of plot B5 is the lowest, i.e., 0.90 $\text{t} \cdot \text{km}^{-2} \cdot \text{a}^{-1}$, and the annual accumulation rate of plot C3 is the highest, i.e., 441.53 $\text{t} \cdot \text{km}^{-2} \cdot \text{a}^{-1}$. The average annual accumulation thickness of all plots is 0.001–0.298 $\text{mm} \cdot \text{a}^{-1}$, and the annual average accumulation modulus is 0.90–441.53 $\text{t} \cdot \text{km}^{-2} \cdot \text{a}^{-1}$.

The $^{210}\text{Pb}_{ex}$ activities in plots A2, A5, B2, C1, C3, C4, D2, D4, E1, and E2 are

5143 ± 662.26 and $7713 \pm 393.57 \text{ Bq/m}^2$, and PPIs are less than the PRI, indicating soil erosion processes. Among these plots, the ^{210}Pb activity of plot D2 is the lowest, representing the largest erosion rate, and the activity of plot C3 is the highest, representing the lowest erosion rate. The average annual erosion thickness of the plots varied between $0.048\text{--}0.536 \text{ mm}\cdot\text{a}^{-1}$, and the annual average erosion modulus ranged between $74.70\text{--}797.98 \text{ t}\cdot\text{km}^{-2}\cdot\text{a}^{-1}$.

4.3 Change in the erosion/accumulation modulus

Generally, $^{210}\text{Pb}_{\text{ex}}$ is believed to be a soil tracer with a very stable sedimentation process, and the soil erosion rate estimated by $^{210}\text{Pb}_{\text{ex}}$ reflects a long-term process (100-year scale) (Mabit *et al.*, 2008). The deposition of the ^{137}Cs tracer mainly occurred in the 1950s and 1970s, and it roughly depicts the soil erosion process since the 1970s (i.e., approximately 50 years ago) (Sun, 2014). Therefore, the soil erosion estimation method using the $^{210}\text{Pb}_{\text{ex}}$ tracer is normally applied to determine the erosion modulus on the 100-year scale, and the method using the ^{137}Cs tracer is usually used to determine the soil erosion modulus on the 50-year scale. Based on a simple inversion formula, the moduli of soil erosion/accumulation in two periods over the past 100 years (the first 50 years and the last 50 years) can be estimated. The results are shown below (Figure 4):

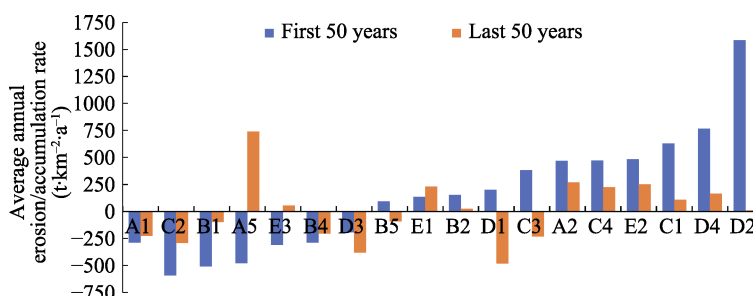


Figure 4 Soil erosion/accumulation modulus in two periods. A positive value indicates erosion, and a negative value indicates accumulation.

In the past 100 years, a total of 5 plots (A1, B1, B4, C2, and D3) have always been in an accumulation state. For plot D3, the accumulation rate increased from $192.65 \text{ t}\cdot\text{km}^{-2}\cdot\text{a}^{-1}$ to $380.85 \text{ t}\cdot\text{km}^{-2}\cdot\text{a}^{-1}$. The accumulation rates of all the other plots have decreased during the past 100 years.

There are 8 plots (A2, B2, C1, C4, D2, D4, E1, and E2) that have always been in an erosive state. The erosion modulus of most plots decreased, but in plot E1, the erosion modulus increased from 134.80 t/km^2 to 231.16 t/km^2 . The change in the erosion rate of plot D2 was significant, and the rate decreased by 99.42%.

Additionally, in 5 plots (A5, E3, B5, C3, and D1), the erosion or accumulation state switched between the two periods. Among these plots, 2 plots (A5 and E3) changed from an accumulation state in the first 50 years to an erosion state in the last 50 years. The other 3 plots (B5, C3, and D1) changed from an erosion state in the first 50 years to an accumulation state in the last 50 years. Moreover, except for plots A5 and D1, the erosion or deposition rates of the other 3 plots were lower in the last 50 years than in the first 50 years.

Based on an analysis of the changes in soil erosion/soil accumulation status and modulus change, the authors conclude that in the past 100 years, the intensity of soil erosion and sandstorm activity has been alleviated. The erosion modulus and accumulation modulus have significantly decreased in most plots, and the other plots change from the erosive state

to the accumulative state. All these facts indicate that the sandstorm activity has significantly weakened, sand fixation has increased, and the regional ecological environment has obviously improved.

5 Discussions

5.1 Uncertainty in the CRI determination

Determining the ^{137}Cs background plots is closely related to the establishment of accurate reference inventories of CRI and PRI. These inventories are crucial for the subsequent judgement of the soil erosion/accumulation state and the quantitative estimation of the erosion/accumulation modulus. The uncertainty in the determination of the ^{137}Cs reference inventory mainly involves the following two aspects: the accuracy of the test instrument and the reliability of the background plot selection, which mainly influences the shape of the ^{137}Cs distribution curve.

First, as a product derived from atmospheric nuclear explosions in the 1950s and 1970s, the ^{137}Cs tracing technique is short of a single source and a short half-life. Therefore, the ^{137}Cs particles in the soil have decreased largely, and they are becoming increasingly difficult to detect with the current instruments. The detection error is increasing, and the accuracy of the calculated CRI is decreasing as well. In addition, in plot B4 (returning farmland), the ^{137}Cs distribution in the vertical profile was interrupted, which may be related to the unknown technical error of the instrument or confused test samples.

Second, ^{137}Cs particles settled to the surface soil and were then redistributed through the migration of soil particles. The distribution pattern of ^{137}Cs in the early background plots showed a typical negative exponential curve. In the later stage, due to the infiltration effect of ^{137}Cs particles, the distribution pattern involving “a single peak + a negative exponential curve” occurred and became common. However, regardless of the distribution pattern, confusion can be caused by the ^{137}Cs distribution patterns of eroded or accumulated plots. That is, in an eroded plot, as the surface soil is denuded, the distribution of ^{137}Cs in the residual soil continues to show a negative exponential curve. In an accumulated plot, the ^{137}Cs distribution may also retain a single peak and negative exponential curve with the low amount of ^{137}Cs that accumulated in the later accumulation stage. Therefore, discrimination error is possible if the tracer distribution pattern is simply observed.

In this paper, a more conservative approach is proposed and developed. i.e. By considering the long-term land use and land cover change history, the potential range of CRI according to the model estimate, and the morphological characteristics of the ^{137}Cs profile, the comprehensive method to judge the background plot is elected first. In this paper, three plots with 3 suites of layer samples and 9 full-profile samples were selected, and the regional CRI and statistical variation were then computed. The comprehensive analysis and statistical calculation method helps to reduce the uncertainty of the CRI estimation.

5.2 Uncertainty of the PRI determination

Generally, the uncertainty in the determination of the $^{210}\text{Pb}_{\text{ex}}$ reference plots and reference inventory is greater.

First, the ^{210}Pb measurement process is more complicated. The calculation of $^{210}\text{Pb}_{\text{ex}}$ needs to consider multiple decay processes, including ^{226}Ra , ^{222}Rn , and ^{238}U . The $^{210}\text{Pb}_{\text{ex}}$ rebalancing process is also a key factor for accurate measurement. These processes may re-

sult in a reduction of the estimation accuracy of the PRI.

Regarding the theoretical estimate of PRI, Chen *et al.* (2013) applied the relationship between regional annual precipitation and the isotope content to establish a dynamic equilibrium model to estimate the $^{210}\text{Pb}_{\text{ex}}$ reference inventory. However, compared with the ^{137}Cs reference inventory estimation model proposed by Walling *et al.*, the application of this estimation model is rare in practical studies. The spatial differentiation of $^{210}\text{Pb}_{\text{ex}}$ distribution in large-scale areas is generally believed to be extremely large, and the $^{210}\text{Pb}_{\text{ex}}$ reference inventory in the eastern part of the Eurasia continent is much higher than that in the western part (Appleby and Oldfield, 1992; Zhang *et al.*, 2003), and the estimation of the RPI using only precipitation data may introduce greater uncertainty.

In this study, a high probability of misjudgment in the $^{210}\text{Pb}_{\text{ex}}$ reference plots was found solely based on the profile distribution of $^{210}\text{Pb}_{\text{ex}}$. Figure 5 shows that all the potential background plots have a negative exponential curve distribution, which is consistent with the distribution pattern of the $^{210}\text{Pb}_{\text{ex}}$ reference plot considered by the general research (Zhang *et al.*, 2003; Li *et al.*, 2009). However, further statistical analysis of the PPI on these potential reference plots shows that the PPIs of these plots vary greatly, with a maximum and minimum difference of 6880 Bq/m^2 , and the coefficient of variation for all samples is 48.3%. Thus, discriminating PRI simply based on the $^{210}\text{Pb}_{\text{ex}}$ distribution pattern is not feasible.

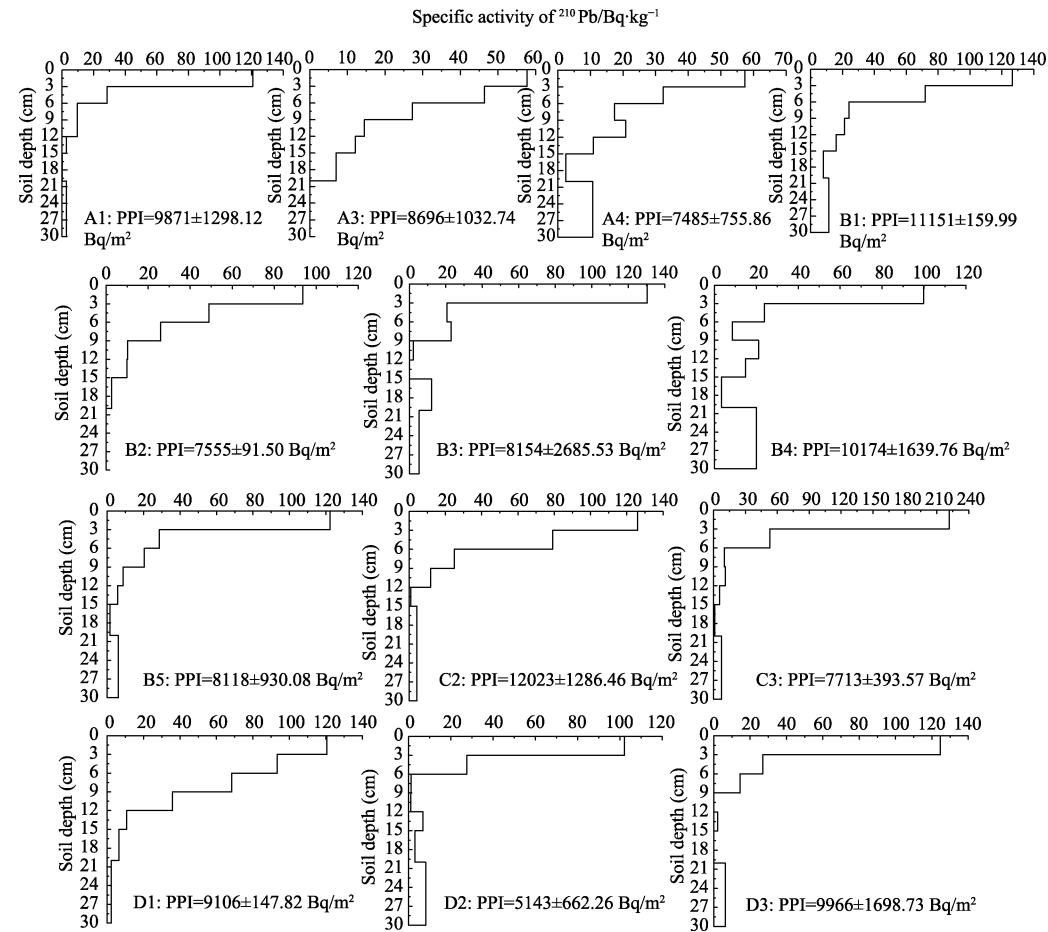


Figure 5 Vertical distributions of $^{210}\text{Pb}_{\text{ex}}$ and PPIs in potential background plots

In summary, the method adopted in this paper is based on the judgment of the nature of the reference plots by ^{137}Cs to help determine the $^{210}\text{Pb}_{\text{ex}}$ reference plots. However, the risks associated with this approach are as follows: the background plots for the short-term erosion process (i.e., determined by the ^{137}Cs allocation process) may not be effective background plots for the long-term erosion process (for the $^{210}\text{Pb}_{\text{ex}}$ allocation process). A given sampling plot may have experienced erosion (or accumulation) in the early stage (i.e., the first 50 years) and then remained stable throughout the late stage (i.e., the last 50 years); consequently, in either case, there would be a bias in the PRI estimate. Compared with the results of previous studies in North China (6128 Bq/m^2) (Hua *et al.*, 2005), the Loess Plateau (5730 Bq/m^2) (Zhang *et al.*, 2003), and Heilongjiang (6600 Bq/m^2) (Wang, 2010), the PRI estimated by this study is likely to be too large. The consequence is that the estimation of the soil erosion modulus may be higher than the true value, while the estimation of the soil accumulation rate may be lower.

6 Conclusions

This paper selects the hilly sandy grassland in Zhenglan Banner, the southern margin of the Hunshandake Sandy Land, as the study area. In this area, reference plots are difficult to determine using only single-isotope tracer techniques, and the estimates of the soil erosion modulus are quite different in different regions and locations. A multi-isotope (^{137}Cs and $^{210}\text{Pb}_{\text{ex}}$) composite tracing technique was developed, and the soil erosion/accumulation moduli and their dynamic changes were analyzed. The uncertainty in the composite isotope tracing technique was discussed. The main conclusions are as follows:

(1) The regional ^{137}Cs and $^{210}\text{Pb}_{\text{ex}}$ reference plots were determined; the regional ^{137}Cs reference inventory was $2123.5 \pm 163.94 \text{ Bq/m}^2$, and the regional $^{210}\text{Pb}_{\text{ex}}$ reference inventory was $8112 \pm 1787.62 \text{ Bq/m}^2$.

(2) Based on the ^{137}Cs tracer analysis, the average erosion thickness ranged from -0.341 to $0.503 \text{ mm} \cdot \text{a}^{-1}$, and the erosion modulus ranged from -48.99 to $740.31 \text{ t} \cdot \text{km}^{-2} \cdot \text{a}^{-1}$. Based on the $^{210}\text{Pb}_{\text{ex}}$ tracer analysis, the average wind-driven soil erosion thickness was -0.298 to $0.536 \text{ mm} \cdot \text{a}^{-1}$, and the erosion modulus was -441.53 to $797.98 \text{ t} \cdot \text{km}^{-2} \cdot \text{a}^{-1}$.

(3) Over the past 100 years, 5 plots have been consistently in an accumulation state, 8 plots have been consistently in an erosion state, 2 plots have changed from an accumulation state to an erosion state, and 3 plots have changed from an erosion state to an accumulation state. In general, the erosion/accumulation rate has decreased significantly over time. Thus, the sandstorm activity has significantly weakened, and the quality of the regional ecological environment has improved.

(4) Regarding the study of isotope tracing techniques, the selection of reference plots of ^{137}Cs and $^{210}\text{Pb}_{\text{ex}}$ and the development of a reference inventory estimation model have an important influence on the judgment of soil erosion and accumulation processes and the calculation of erosion rates. On the one hand, a comprehensive investigation should be carried out based on historical land cover and land use changes, on-site environment observation, theoretical model estimation, and the isotope distribution. On the other hand, the application of multi-isotope composite techniques can help overcome the problem of easily misjudged reference plots and help to reduce the estimation uncertainty.

References

Appleby P G, Oldfield F, 1992. Applications of lead-210 to sedimentation studies. *Uranium-series Disequilibrium*:

- Applications to Earth, Marine, and Environmental Sciences*, 25(22): 731–738.
- Baskaran M, 2016. Progeny of Radon (^{210}Pb) as a Tracer and Chronometer in Continents and Aqueous Systems. Radon: A Tracer for Geological, Geophysical and Geochemical Studies. Springer, 145–166.
- Chappell A, Sanderman J, Thomas M *et al.*, 2012. The dynamics of soil redistribution and the implications for soil organic carbon accounting in agricultural south-eastern Australia. *Global Change Biology*, 18(6): 2081–2088.
- Chen R T, Zhang M L, Yang H, 2013. Dynamic equilibrium model of $^{210}\text{Pb}_{\text{ex}}$ background value in soil. *Research of Soil and Water Conservation*, 20(5): 73–76. (in Chinese)
- Evans R, Collins A, Zhang Y *et al.*, 2017. A comparison of conventional and ^{137}Cs -based estimates of soil erosion rates on arable and grassland across lowland England and Wales. *Earth-Science Reviews*, 173: 49–64.
- Feng T, Chen H S, Zhang W *et al.*, 2011. ^{137}Cs profile distribution character and its implication for soil erosion on karst slopes of Northwest Guangxi. *Chinese Journal of Applied Ecology*, 22(3): 593–599. (in Chinese)
- He J, Wu X H, Yang T T *et al.*, 2015. The sand grain diameter composition of quicksand and its contiguous grassland in Hunshandake sandy land in growth season. *Journal of Arid Land Resources and Environment*, 29(1): 95–99. (in Chinese)
- Hu J F, Sha Z J, Ma Y J *et al.*, 2017. Technical principle of $^{210}\text{Pb}_{\text{ex}}$ tracer method and its application in soil erosion. *Journal of Salt Lake Research*, 25(1): 76–80. (in Chinese)
- Hu Y F, Liu J Y, Batu N C *et al.*, 2014. Determination of ^{137}Cs reference inventories in a large-scale region: A case study in the central-eastern Inner Mongolia Plateau. *Journal of Geographical Sciences*, 24(6): 1047–1059.
- Hua L, Zhang Z G, Li J B *et al.*, 2005. Soil erosion and organic matter loss by using fallout ^{137}Cs as tracer in Miyun reservoir valley. *Acta Agriculturae Nucleatae Sinica*, 19(3): 208–213. (in Chinese)
- Li J J, Li Y, Wang Y L *et al.*, 2009. Study of soil erosion on the East-West transects in the Three-Rivers Headwaters region using ^{137}Cs and $^{210}\text{Pb}_{\text{ex}}$ tracing. *Research of Environmental Sciences*, 22(12): 1452–1459. (in Chinese)
- Li J Y, Xu B, Yang X C *et al.*, 2011. Dynamic changes and driving force of grassland sandy desertification in Xilin Gol: A case study of Zhenglan Banner. *Geographical Research*, 30(9): 1669–1682. (in Chinese)
- Li P, Yang T T, Wu X H *et al.*, 2013. Climate Change in Zhenglan Banner, Inner Mongolia in Recent 40 Years. *Arid Zone Research*, 30(5): 776–780. (in Chinese)
- Li S, Lobb D A, Kachanoski R G *et al.*, 2011. Comparing the use of the traditional and repeated-sampling-approach of the ^{137}Cs technique in soil erosion estimation. *Geoderma*, 160(3/4): 324–335.
- Liu J Y, Qi Y Q, Shi H D *et al.*, 2007. Estimation of wind erosion rates by using ^{137}Cs tracing technique: A case study in Tariat-Xilin Gol transect, Mongolian Plateau. *Chinese Science Bulletin*, 53(9): 2785–2791. (in Chinese)
- Liu Y, Lv Y H, Fu B J *et al.*, 2010. Reference value of ^{137}Cs tracing technique in soil loss estimation: A spatial variation analysis. *Geographical Research*, 29(7): 1171–1181. (in Chinese)
- Mabit L, Benmansour M, Walling D E, 2008. Comparative advantages and limitations of the fallout radionuclides ^{137}Cs , $^{210}\text{Pb}_{\text{ex}}$ and ^7Be for assessing soil erosion and sedimentation. *Journal of Environmental Radioactivity*, 99(12): 1799–1807.
- Nan L, Du L T, Zhang X L, 2014. Advances in study on soil erodibility for wind erosion. *Soils*, 46(2): 204–211. (in Chinese)
- Porto P, Walling D E, Callegari G, 2011. Using ^{137}Cs measurements to establish catchment sediment budgets and explore scale effects. *Hydrological Processes*, 25(6): 886–900.
- Qi Y Q, Liu J Y, Shi H D *et al.*, 2008. Using ^{137}Cs tracing technique to estimate wind erosion rates in the typical steppe region, northern Mongolian Plateau. *Chinese Science Bulletin*, 53(9): 1423–1430. (in Chinese)
- Qi Y Q, Zhang X B, He X *et al.*, 2006. ^{137}Cs reference inventories distribution pattern in China. *Nuclear Techniques*, 29(1): 42–50. (in Chinese)
- Sun W, 2014. Modeling research on estimating soil erosion rates using lead-210, beryllium-7, and cesium-137 and numerical simulation [D]. Nanjing: Nanjing Normal University. (in Chinese)
- Sun W, Yang H, Zhao Q G *et al.*, 2013. Response model of $^{210}\text{Pb}_{\text{ex}}$ content in non-arable soil to change of erosion rate. *Chinese Science Bulletin*, 58(15): 1379–1384. (in Chinese)
- Sutherland R A, 1998. The potential for reference site resampling in estimating sediment redistribution and assessing landscape stability by the caesium-137 method. *Hydrological Processes*, 12(7): 995–1007.
- Walling D E, He Q, 2000. Final Report on IAEA Technical Contract 10361/RO-R1. University of Exeter, 11.
- Wang Y, 2010. Investigating the soil erosion rates on the cultivated slopes in the northeast black soil region of China using ^{137}Cs and $^{210}\text{Pb}_{\text{ex}}$ measurements [D]. Xi'an: Graduate University of Chinese Academy of Sciences, Institute of Soil and Water Conservation. (in Chinese)
- Winkelbauer J, Völkel J, Leopold M *et al.*, 2012. The vertical distribution of Cs-137 in Bavarian forest soils. *European Journal of Forest Research*, 131(5): 1585–1599.
- Zhang W, Pan S M, Zhang K X *et al.*, 2015. Study of the Cesium-137 Reference Inventory in the Mainland of China. *Acta Geographica Sinica*, 70(9): 1477–1790. (in Chinese)
- Zhang X B, Higgitt D L, Walling D E, 1990. A preliminary assessment of the potential for using caesium-137 to estimate rates of soil erosion in the Loess Plateau of China. *Hydrological Sciences Journal*, 35(3): 243–252.
- Zhang X B, Quine T A, Walling D E *et al.*, 1994. Application of the caesium-137 technique in a study of soil erosion on gully slopes in a yuan area of the Loess Plateau near Xifeng, Gansu Province, China. *Geografiska Annaler: Series A, Physical Geography*, 76(1/2): 103–120.
- Zhang X B, Wang D E, Feng M Y *et al.*, 2003. The depth distribution of $^{210}\text{Pb}_{\text{ex}}$ in soil and soil erosion rate model by $^{210}\text{Pb}_{\text{ex}}$ method. *Chinese Science Bulletin*, 48(5): 502–506. (in Chinese)